https://doi.org/10.1016/j.jpowsour.2019.227549

Chemical Bonding Black Phosphorus with TiO_2 and Carbon toward High-Performance Lithium Storage

Fengchen Zhou[a], Liuzhang Ouyang[a,b*], Jiangwen Liu[a], Xu-Sheng Yang[c,d*], Min Zhu[a]

[a] School of Materials Science and Engineering, Guangdong Provincial Key Laboratory of Advanced Energy Storage Materials, South China University of Technology, Guangzhou, 510641, China. Email: meouyang@scut.edu.cn

[b] China-Australia Joint Laboratory for Energy & Environmental Materials, Key Laboratory of Fuel Cell Technology of Guangdong Province, Guangzhou, 510641, China

[c] Advanced Manufacturing Technology Research Centre, Department of Industrial and Systems Engineering, The Hong Kong Polytechnic University, Hung Hom, Kowloon, Hong Kong, China. Email: xsyang@polyu.edu.hk

[d] Hong Kong Polytechnic University Shenzhen Research Institute, Shenzhen 518057, China

[*]Corresponding authors.
[a*] E-mail: meouyang@scut.edu.cn, (L. Ouyang)
[c*] E-mail: xsyang@polyu.edu.hk, (X. Yang)

Abstract

Phosphorus (P)-based materials are recognized as one type of prospective candidate anodes due to its high theoretical capacities. However, it still suffers the relatively low structural stability and rate performance. In the present work, an amorphous ternary black Phosphorus (BP)- Titanium dioxide (TiO_2)- Carbon (C) nanocomposite is fabricated by a facile ball milling process, which can serve as a prospective alternative for advanced anode material of Lithium-Ion Battery (LIB). We find that the introduction of TiO_2 can effectively improve the conductivities of electron and lithium ion, the electrode reaction kinetics, and stabilize the structural integrity of the active material. What's more, the strong Ti-O-P bonds, forming among TiO_2 and BP, can further improve the utilization of active material and the transfer of interfacial electron. As a result, the BP-TiO_2-C composite exhibits outstanding electrochemical performance, involving high specific capacity, excellent rate performance (a reversible capacity of 947.4 mAh g^{-1} at 7.0 A g^{-1}), and stable cycling performance (a capacity of 935.8 mAh g^{-1} after 300 cycles at 2 A g^{-1} with 85.3% retention ratio). Furthermore, when this nanocomposite is assembled with $LiCoO_2$ cathode to build a full cell, it can also denote an excellent specific capacity, stable cycling performance and rate performance.

Keywords: Black phosphorus; TiO_2; Ti-O-P bond; synergistic effect; lithium ion battery

1. Introduction

With the growing demand of large-scale stationary energy storage and various types of electric vehicles, the energy storage materials such as lithium-ion batteries (LIBs) with higher capacity, energy density and longer lifespan, etc., are highly required to be developed [1, 2]. Phosphorus (P) with high theoretical capacity (2596 mAh g^{-1}, i.e., seven times as high as conventional graphite) enter researchers' perspective to meet these requirements. In addition, the suitable operating potential (i.e., ~ 0.7 V vs. Li^+/Li) of P anode materials can effectively inhibit the growth of the metallic lithium plating [3-6]. Notably, the black P (BP) with layered structure denotes the best thermodynamically stability allotrope of phosphorus at room temperature. Compared to the size of lithium and sodium ions, which are 1.52 Å and 2.04 Å, respectively, more specifically, the BP with much larger interlayer channel size of 3.08 Å can contribute to the rapid Li^+/Na^+ diffusion along the zigzag direction [7, 8]. However, like Si, Sn, Ge and SnO_2 anodes, BP anode still faces some other problems, e.g., the rapid capacity fading and electrical contact losing that are mainly caused by huge volume change (~ 300%) from BP to Li_3P [3]. Additionally, it still suffers unfavorable reversible electron transport for batteries, although with high electrical conduction (10^2 S m^{-1}). Thus, how to improve structural stability and conductivity of the BP anode material has become an essential factor to promote the development of high-energy BP-based LIBs.

Two different kinds of approaches, i.e., reducing the particle size [9-11] and fabricating conductive matrix [3, 7, 12-15], have been widely adopted to address above

mentioned issues. The former approach can shorten the ion diffusion paths and thus improve its electrochemical properties, but it cannot avoid the huge volume change during charge/discharge cycle. The later approach via fabricating BP with the conductive carbon matrix is much more promising due to the significant improved electrochemical performance at following several aspects. Firstly, the carbon matrix can enhance the conductive of electron and improve the kinetics of the electrochemical reaction.[6] Furthermore, the large volume change-induced mechanical stress can be alleviated during cycling by carbon matrix, and so as the increased stability of the electrode structure. Thirdly, carbon matrix can also prevent the BP particle direct contacting electrolyte, which produces a stable solid electrolyte interphase (SEI) film. Nonetheless, the relatively low ionic conductivities of BP and carbon matrix are still existed in this approach, highly weakening its electrochemical property, especially the rate capacity. Therefore, it is essential to find an effective strategy to enhance the fast Li^+ ion transfer in BP material, and then improve the capacity and cycle performance at high rates.

Anatase TiO_2 is generally considered to be an excellent anode material, due to its outstanding thermal stability and structural stability to electrolyte, and slight volume change (< 4 %) in the LIBs systems [16]. Notably, TiO_2 can exhibit a rapid Li^+ migration along (001) plane [17, 18]. In addition, TiO_2 shows an increase of electric conductivity after lithiation because the Ti^{3+} and Ti^{4+} valence states coexist in the LIBs systems (Li_xTiO_2, $0 \leq x \leq 1$) [17, 19]. Therefore, TiO_2 has been also widely used to form some TiO_2-related nanocomposites for achieving the high-performance LIBs

anodes [19, 20]. For example, 1D SnO_2-amprohous TiO_2 nanotubes (NTs) composite and the incorporation of TiO_2 component in SiOx-TiO2@C nanocomposite were respectively synthesized to denote the excellent cycle retention and rate capabilities, and the effectively enhancement of the conductivities of electron and lithium ion of the SiOx particles [19, 20]. Particularly, Song et al. introduced the BP into TiO_2 to form TiO_2-BP-S composite with 20 wt% BP and 80 wt% TiO_2, producing the stable P-S bonds with sulfur and strong P-Ti bonds with TiO_2 [21]. It turned out that the stable P-S and P-Ti bonds can enhance the specific capacity and electrical conductivity of TiO_2-BP-S composite, thus solving the drawbacks of TiO_2-based anodes for SIBs systems and reducing the large volumetric expansion of formed Na_3P. It has been certified that chemical bonds (P-C and P-O-C) can enhance the electrochemical performance of P-based material in both lithium/sodium-ion storage systems [5, 7, 9, 22]. These strong chemical bonds can help maintain the electrical connection between carbon and phosphorus, restrain the volume expansion during cycle, and thus stabilize the structure. Along this line of thought, introduction of TiO_2 into BP-C to construct BP-TiO_2-C ternary composite could also have chance to form a certain strong chemical bonding among TiO_2 and BP, thus donating an effective strategy to simultaneously facilitate the ionic and electronic conductivities, increase the electrical contact and structural stability of BP-C electrode for LIBs system. According to the best of our knowledge, however, there is still quite limited literatures regarding the ternary BP-TiO_2-C composite as the high-performance LIBs anode materials, which will be achieved in the present work.

Herein, we report a productive and efficient route to synthesize one typical amorphous BP-TiO_2-C nanocomposite towards high-performance LIBs anode via a scalable ball milling method. The fabricated amorphous BP-TiO_2-C nanocomposite has extreme tiny TiO_2 nanoparticles that disperse into the amorphous BP and carbon nanoparticles, which are anchored on the expanded graphite. The experimental analyses reveal that TiO_2 transformed into Li_xTiO_2 phase during the first discharging processes could intrinsically enhance the lithium ions and electrons migration within BP-TiO_2-C composite. Meanwhile, the carbon matrix could also promote the electronic conduction and buffer the stress produced by the large volume expansion of BP component. Furthermore, the strong covalent interaction (Ti-O-P bonds) formed at interfaces between BP and TiO_2 can be beneficial to the electron transfer of the composite interfaces and its structural stability. Thus, the BP-TiO_2-C nanocomposite exhibits superior electrochemical performance, e.g., high reversible capacities and stable cycling stabilities, and especially the excellent rate capacities. In addition, a reversible capacity as high as 935.4 mAh g^{-1} can be maintained, denoting a capacity retention of 85.3%, even after cycled 300 charge/discharge times at 2 A g^{-1}. The experimental results of the present work indicate a novel strategy for developing the phosphorus-based anode material of LIBs with high electrochemical performance.

2. Experimental section

2.1 Preparation of BP-TiO_2-C composite

The BP-TiO_2-C was prepared from the raw materials of BP, anatase TiO_2 and expandable graphite (EG) by one-step simple ball milling method, as schematically

shown in Fig. 1a. The synthesized methods of BP and EG were the same as our previous reported works [23]. BP, TiO_2 and EG with different weight ratios of 5:2:3, 5:1:4 and 6:2:2 were respectively milled for 5 h with the high-energy shake milling equipment (QM-3C supplied by the company of Nanjing Nada Instrument Co. Ltd.) at argon atmosphere. The ball-to-power ratio was selected to be 50:1 with the ball milling rotation rate of 1200 rpm. On the basis of the preliminary electrochemical test results (Fig. S1), the optimum weight ratio was found to be 5:2:3. Therefore, all of the experiments conducted and data discussed in the present work refer to the BP-TiO_2-C composite with weight ratio of 5:2:3, unless otherwise specified. For comparison, the BP-C composite was also synthesized with a weight ratio of 5:5 without TiO_2 addition under the same conditions.

2.2 Materials characterization

X-ray diffraction (XRD) profiles data for identifying the phase constitutes of the samples were seek from a PANalytical Empyrean with Cu Kα radiation. Functional groups and bond features were characterized by Fourier-transform infrared spectroscopy (FTIR). Renishaw RM2000 confocal Raman microscopes (with the excitation laser of 532 nm) were used to obtain the Raman spectra. Besides, X-ray photoelectron spectroscopy (XPS) spectra was collected from a Thermo Scientific ESCALAB 250. The morphologies were analyzed by scanning electron microscopy (SEM with category of Carl Zeiss Supra 40), and the detailed microstructure, including interplanar spacing, were further characterized by using the transmission electron microscopy (TEM; JEOL JEM-2100) that was operated at voltage of 200 kV.

2.3 Electrochemical characterization

First, 70 wt% active material, 15 wt% carboxymethyl cellulose and 15 wt% Super P, respectively, in weight were first mixed homogenously. It was then coated on a copper foil for providing the working electrodes. The active material had the value ~0.6 mg cm^{-2} in mass loading. The lithium foils were used as the counter electrode to assemble the test cells in a glove box filled by argon atmosphere. Electrolyte was set up via dissolving the 1 M $LiPF_6$ into a mixture of EC/DEC/DMC (1/1/1, v/v/v) with the addition of 10 wt% FEC. Charge-discharge test of the nanocomposite was conducted on a battery test system (LAND CT2001A), possessing the 0.01-2.00 V (vs. Li^+/Li) voltage window. Electrochemical impedance spectroscopy (EIS, frequency between 100 kHz to 0.01 Hz) with 5 mV AC signal amplitude was measured from electrochemistry workstation (Gamry Interface 1000). Cyclic voltammetry (CV) curves were obtained from the electrochemistry workstation at 0.1 mV s^{-1} between 0.01–2.00 V. The cycled electrodes for the SEM and XPS observations were prepared by disassembling the test cells, cleaning with DEC and drying for several days in the glove box filled by argon atmosphere. Full cells were set up by respectively paring with commercial $LiCoO_2$ electrode as cathode and BP-TiO_2-C nanocomposite electrode as anode. The $LiCoO_2$ electrode consisted active materials, super P and polyvinylidene fluoride with weight ratio of 80:10:10. The CV curves of the full cell were measured among 2.00 and 3.90 V at 0.1 mV s^{-1}. The voltage window of galvanostatic discharge/charge tests of the full cell was 2.00-3.90 V (vs. Li^+/Li). According to the composites weight, we calculated the current densities and the specific capacities.

3. Results and discussion

3.1 Structure of the BP-TiO_2-C composites

The overall synthesized process of the BP-TiO_2-C composites is shown in Fig. 1a. Particularly, the BP, TiO_2 and EG are connected by the bonds (P-C bonds, P-O-C bonds and Ti-O-P bonds) that will be experimentally confirmed in the following experimental characterizations. Fig. 1b gives the XRD patterns to study the compositions and structures of BP-TiO_2-C, BP-C and BP, respectively. It is noted that all the diffraction peaks of the raw material BP can be identified well with that of standard pattern of BP with JCPDS No. 73-1358 [24, 25]. However, no obvious diffraction peak of BP is found from the XRD patterns of BP-TiO_2-C and BP-C, which might indicate that the BP became amorphous after ball milling with EG or EG and TiO_2 and it will be evented by the TEM observations in the next section in the present work. The intense diffraction peaks at 26.5° in composite samples can be indexed to be the (002) of graphite from EG. The XRD pattern of the BP-TiO_2-C composite only shows the diffraction peaks of graphite and TiO_2, without any other diffraction peak. It indicates that there is no new phase generated from the BP and TiO_2 during ball milling. The Raman spectra of BP-TiO_2-C, BP-C, EG, and BP are respectively shown in Fig. 1c, where both of BP-TiO_2-C and BP-C composites show no Raman peak for P and only carbon peaks exist at 1346 and 1594 cm^{-1} for D and G bands. This might be attributed to that P is covered by carbon in the composites, leading to the significant decrease in the intensity of P peaks [4]. The original magnitude of 0.37 in the intensity ratio of D band to G band (I_D/I_G) in EG is increased to 2.21 in BP-C and 2.28 in BP-TiO_2-C composites, respectively. Besides, the

G band peaks shifted from 1581 in EG to 1594 cm^{-1} in BP-C and BP-TiO_2-C composites could be considered due to the thickness of EG layers is decreased after ball milling [22, 26]. Noticeably, there is an additional peak in BP-TiO_2-C located at 152 cm^{-1}, quite close to the 144 cm^{-1} of Anatase TiO_2 with the anatase structure (E_g mode), owing to the reduced nanoparticle size and surface strain during the ball milling [27, 28]. The surface chemical structures of BP-C and BP-TiO_2-C composites were proved by FTIR spectroscopy in Fig. 1d, from which the peaks at 1160 and 1076 cm^{-1} can be corresponded to P=O and P-O bonds owing to the exposure of P particles in the air. Notably, a peak is found to be at 1008 cm^{-1}, suggesting the existence of P-O-C bond and also the strong interaction between EG and BP [12, 29].

Fig. 2a gives the SEM image of the BP-TiO_2-C composite, showing the irregular nanoparticles with sizes ranged from 100 nm to 500 nm. The TEM and associated HRTEM images of one typical BP-TiO_2-C nanocomposite are respectively given in Fig. 2b-c, exhibiting clearly the existence of TiO_2 nanoparticle with size of several nanometers. Two interplanar spacings are indexed to be 0.238 and 0.352 nm in Fig. 2c, respectively, which refer to the (004) plane and (101) plane of TiO_2 nanoparticle. It should be noted that these TiO_2 nanoparticles are surrounded by the BP matrix with amorphous structure. The phase structure of BP-TiO_2-C nanocomposite agrees well with the XRD results as shown in Fig. 1b. Furthermore, elemental mapping analysis in Fig. 2d1-d4 was employed to exhibit the distribution of P, C, Ti, and O of BP-TiO_2-C nanocomposite given in Fig. 2b, indicating the homogeneous distribution of P, C, Ti, and O elements. However, the O element mapping is slightly weaker than that of Ti,

possibly owing to the potential partial reduction of TiO_2 during the synthesized process. The HRTEM image of BP-C nanocomposite, as shown in Fig. S2, exhibits clearly the presence of graphite structure, as the indexed (101) plane interplanar spacing of 0.208.

Furthermore, Fig. 3a-d presents the C 1s, P 2p, O 1s, and Ti 2p XPS spectra, respectively, to analyze the chemical state of BP-TiO_2-C composite and the interaction among BP, TiO_2 and EG. Besides, the C 1s, P 2p, and O 1s XPS spectra of the BP-C composite are given in Fig. S3. The C 1s XPS spectra in Fig. 3a can be fitted to five peaks. In details, the peaks located at 284.7 eV and 285.4 eV are corresponded to C-C bond with sp^2 and sp^3 hybrid orbital, and the peak observed at 288.3 eV is ascribed to the C=O bond. The peak located at 284 eV should be assigned to the C-P bond [5, 30]. And the peak located at 286.1 eV should be contributed to the C-O-P bond [31], which agrees with the FTIR results. The P 2p XPS spectra can be first fitted with two pairs of $2p_{1/2}$ and $2p_{3/2}$. A couple of peaks centered at 129.9/130.7 eV is assigned to the P-P bond, on the contrast, another couple located at 130.3/131.1 eV is ascribed to P-C bond [5, 30]. In addition, the peak appeared at 133.8 eV in Fig. 3b is corresponded to the P-O bond, caused by slight oxidation of raw RP. The O 1s XPS spectra in Fig. 3c shows the characteristic peaks of C=O (533.5 eV), C-O-P (532.6 eV), P-O (532.0 eV), P=O (531.0 eV) and Ti-O-Ti (530.5 eV). Particularly, the peak appeared at $\approx$531.3 eV corresponds to Ti-O-P bond, meaning that the bridging oxygen bonds are formed among the BP and TiO_2 [9, 32]. During the high-power ball milling process, the interface temperature of material would be increased significantly by the intensive collisions between the balls. In consequence, the hydroxyl groups on the surface of BP can react with the bridging

hydroxyl groups of the TiO_2 to form the Ti-O-P bonds [33]. Furthermore, the P atoms can diffuse into the TiO_2 lattice, replace the Ti^{4+} sites and connect with cataclastic TiO_2 via forming Ti-O-P bonds [33]. Fig. 3d shows the Ti 2p XPS spectra of the BP-TiO_2-C. Both peaks of Ti^{4+} at 459.7 and 465.3 eV originating from TiO_2 and Ti^{3+} at 459 and 464.3 eV can be well indexed. With increasing temperature of the interface, the BP and EG can serve as a reductant for reducing the fractured TiO_2 surface. More specifically, the P^{5+} replaced the Ti^{4+} sites can also result in the deficiency of lattice oxygen from the TiO_2. Such composite valence states of Ti are advantageous to the electron transfer in BP-TiO_2-C composite [17, 19]. Noticeably, the spectra of Ti 2p XPS shifts negatively by ≈ 1 eV, compared with the previous research works [32, 34], which would be due to the strong interaction between the BP and TiO_2 with Ti-O-P bands.

3.2 Electrochemical Lithium Storage Performance

Electrochemical performances of the BP-TiO_2-C and BP-C composites as anode materials of LIBs were investigated. Fig. 4a first shows the measured results of cyclic voltammetry (CV) curves of BP-TiO_2-C electrode to examine the electrochemical behavior. The peak apparently observed at 0.56 V is ascribed to the lithiation process with BP for forming Li_yP (y = 1-3) [13, 29]. On the anodic scan, the apparent peak at 1.03 V ascribes to the delithiation process of Li_yP. This anodic peak splits into two peaks, close to 1.0 and 1.12 V, respectively, in the subsequent cycles, indicating a stepwise delithiation process from the Li_yP to P [29, 35]. The CV curves of BP-C electrode also exhibits the same trend as shown in Fig. S4. Moreover, CV curves ranged 0.01-3.00 V was measured, as shown in Fig. 4b, to clarify the state of TiO_2 during the

charge/discharge process. The enlarged insert in Fig. 4b exhibits a pair of reduction and oxidation peaks at ~ 1.75 V and 2.05 V, respectively, which are corresponded to the Li^+ insert/extract from anatase TiO_2 [19]. Therefore, Li^+ should be inserted into TiO_2 in the initial discharge process and not be extracted in the charge process with the 0.01-2.00 V (vs. Li^+/Li) potential window. In other words, TiO_2 will exist via the form of Li_xTiO_2 in the composites in the following charge/discharge process after initial charging. Meanwhile, the Li_xTiO_2 displays mixed $Ti^{3+/4+}$ valence, thus possessing a high electronic conductivity in the whole charge/discharge process. Besides, these pair of peaks are relatively weak in intensities, presumably ascribe the low content in BP-TiO_2-C composite. It may be also the reason that why the lithiation process of TiO_2 cannot be easily found in the CV curves with 0.01-2.00 V in Fig. 4a. Above experimental results suggest that the electrochemical reactions mechanism of BP-TiO_2-C composite involved during the charge/discharge process would be as follow:

$TiO_2 + xLi^+ + xe^- \rightarrow Li_xTiO_2$ $(0 \leq x \leq 1)$

$P + yLi^+ + ye^- \leftrightarrow Li_yP$ $(0 \leq y \leq 3)$

$C + nLi^+ + ne^- \leftrightarrow Li_nC_6$

Fig. 5a exhibits the charge-discharge profile of BP-TiO_2-C and BP-C electrodes with the initial cycle at a current density of 500 mA g^{-1}, respectively. The BP-TiO_2-C electrode demonstrates the initial discharge capacity of 1581.1 mAh g^{-1}, slightly higher that of 1525.4 mAh g^{-1} in BP-C. It should be noted that the specific capacities of two samples are calculated according to the total composites weight, i.e., BP + TiO_2 + C and BP + C. The BP-TiO_2-C has a lower theoretical capacity than BP-C, given that two

samples have the same weight of BP, and the lower theoretical specific capacity of TiO_2 than that of expanded graphite. Therefore, the practical higher capacity in BP-TiO_2-C indicates that the introduction of TiO_2 and formation of Ti-O-P bond can improve the electrochemical activity and the utilization of BP. Besides, the initial coulombic efficiency (ICE) of BP-TiO_2-C is 84.19%, slightly lower than that of BP-C (84.37%), due to that the Li^+ cannot extract from Li_xTiO_2. It is also noted that the hysteresis (ΔE_P) of the discharge and charge plateaus of BP-TiO_2-C can be determined to be 0.3V, which is smaller than that of BP-C, even lower than the mixed composited of black P-graphite and black P-Ketjen Black [5, 36]. The improvement directly contributes to the Ti-O-P bond can keep the better connection between particles during the potential volume change induced by charge/discharge process. In addition, the fast Li^+ diffusion along *c*-axis (in the [001] direction) of TiO_2 through vacant octahedral sites can effectively improve the Li^+ diffusion rate in the composite [17, 18].

Fig. 5b shows the cycling properties of the BP-TiO_2-C and BP-C electrodes were measured and compared at a current density of 500 mA g^{-1}. In particular, the ICE of BP-TiO_2-C is 84.19%, and the coulombic efficiency can achieve 99.5% after initial five cycles. After 200 cycles, the reversible capacity of BP-TiO_2-C can maintain at 1026 mAh g^{-1}. For the BP-C electrode, its capacity can only maintain about 130 cycles (1000.6 mAh g^{-1}), and then quickly decline to 680.7 mAh g^{-1} after 200 cycles. These results indicate that the introduction of TiO_2 to BP-C matrix can play a significant part in the improvement of structural stability and electrochemical performance, which might be understood in the following several aspects and it will be evidenced by the

experimental results later in the present work. Firstly, the less volume expansion of TiO_2 during cycling can contribute to absorb the stress and restrain the volume expansion produced by BP [16, 19, 20]. Furthermore, the rapid electron and Li^+ migration in Li_xTiO_2 can enhance the electrochemical reaction kinetics of the BP-TiO_2-C particles. Thirdly, the Ti-O-P bond can promote the utilization of BP, enhance the efficiency of interfacial electron transfer and further improve the structure stability of the composite.

Fig. 5c displays the rate performance of the BP-TiO_2-C and BP-C electrodes ranged between 0.2 to 7 A g^{-1}. With the comparison of BP-C electrode, the BP-TiO_2-C electrode reveals an excellent rate performance. For example, the mean charge capacities of 1207, 1117.6, 1065, 1022.9, 997 and 969.1 mAh g^{-1} can be respectively obtained at 0.2, 0.5, 1.0, 2.0, 3.0 and 5.0 A g^{-1}, much higher than those of BP-C electrode (1199, 1110.4, 1033.4, 921.9, 852.6 and 776 mAh g^{-1}, respectively). A reversible capacity of 947.4 mAh g^{-1} is achieved even the as high as 7.0 A g^{-1} current density, which is about 2.5 times of commercial graphite. More specifically, after the ultrahigh rate cycling, a high specific capacity of 1060.6 mAh g^{-1} can be returned in BP-TiO_2-C electrode once the current density is reversed to 0.5 A g^{-1}. After that, a high capacity of 1035.9 mAh g^{-1} can be obtained if do another 50 cycles at 0.5 A g^{-1}, with 92.7% of the initial capacity, suggesting the excellent rate property and outstanding capacity recovery performance of BP-TiO_2-C material. Compared with the P-based composites in literature, the prepared BP-TiO_2-C electrode in the present work shows excellent rate capability and high specific capacity, as presented in Fig. 4d and Table S1 [10, 12-14, 28, 29, 37-41].

Fig. 5e shows the long cycling property of BP-TiO_2-C electrode at high current

density with initial three cycles at low current density. The BP-TiO_2-C electrode exhibits a high capacity about 935.8 mAh g^{-1} after 300 cycles with 85.3% capacity retention (based on the fourth cycle), indicating an excellent long-term cyclability at high current density. The outstanding electrochemical property indicates a potential promise of the proposed strategy. For comparison, the electrochemical performance of RP-TiO_2-C composite with RP as raw material also investigated as shown in Fig. S5. Although P in the BP-TiO_2-C and RP-TiO_2-C are both amorphous, the BP-based composite demonstrates obviously a better electrochemical performance. The possible reason might be come from that 1) the P, similar to C, H_2O, and silicate glasses is in the polyamorphous state, and 2) the amorphous P formed from BP can keep the higher structural and electronic properties than that of RP or other related RP-based amorphous products [42].

3.3 Electrochemical property of LCO|BP-TiO_2-C full-cell

To showcase the true performance of BP-TiO_2-C, a full LIB cell with BP-TiO_2-C as anode and $LiCoO_2$ (LCO) as cathode was fabricated and its performance is shown in Fig. 6. The full cell was tested between 2.0 to 3.9 V, and the charge/discharge profile at the current density of 500 mA g^{-1} is shown in Fig. 6a. The full cell delivers an initial specific charge/discharge capacity of 1538.6 and 1059.8 mAh g^{-1} (based on the weight of BP-TiO_2-C composite), with an initial coulombic efficiency of 68.88%. The CV curves of full cell measured at 0.1 mV s^{-1} is shown in Fig. 6b. During the initial charging process, the obvious peak at 3.3 V can be assigned to the Li^+ extract from the LCO and react with BP-TiO_2-C. The peak is transited to the left in the following cycles and

caused by the electrode polarization decreases after initial activation. In the cathodic process, two peaks at 2.9 and 2.75 V can be corresponded to the delithiation of Li_3P and lithiation of Li_xCoO_2. The two cathodic peaks indicate the two-step reaction during the discharge process, agreeing with the CV curve of BP-TiO_2-C composite in Fig. 4. The rate capacities of full cell are shown in Fig. 6c. The average charge capacities of 1080.7, 975.7, 924.5, 878, 840.7 and 763.4 mAh g^{-1} can be obtained at 0.2, 0.5, 1.0, 2.0, 3.0 and 5.0 A g^{-1}, respectively. More important, after the ultrahigh rate cycling, a specific capacity as high as 969 mAh g^{-1} can be returned once switches back to 0.5 A g^{-1}, demonstrating the outstanding rate property and excellent recovery capacity. The cycling performance of the full cell tested at the current densities of 500 and 1000 mA g^{-1} are shown in Fig. 6d. The reversible discharge capacity of full cell can maintain at 942.9 mAh g^{-1} (89.2% capacity retention) and 857.6 mAh g^{-1} (88% capacity retention) after 100 cycles, respectively. These results demonstrate that the BP-TiO_2-C nanocomposite has a great potential for the practical application in full cell.

3.4 Structural stabilization mechanism

To further reveal the structure advantages of BP-TiO_2-C electrode to improve the electrochemical performance, the EIS, SEM and XPS of the 100 times cycled electrode at 1.0 A g^{-1} were compared and investigated. Fig. 7a shows the Nyquist plots of these two electrodes measured at 0.01 V. The spectra consist of three typical parts: the first semicircle represents the impedance of the SEI film, the second semicircle ascribes to the transfer of charge, and the inclined line (the third part) corresponds to Li^+ diffusion. An equivalent circuit is given as the inset in Fig. 7a, consisting of the electrolyte

solution resistances (R_e), SEI film resistances (R_f), charge transfer resistances (R_{ct}), and constant phase elements instead of pure capacitance, followed by the Warburg impedance (W_s) [43]. The BP-TiO_2-C electrode has a lower R_{ct} parameter than the BP-C electrode after 100 cycles, which demonstrates the fast electrode reaction kinetic. This may be attribute to the well-diffused Li_xTiO_2 and the Ti-O-P bonds, which facilitate the fast ionic and electronic transfer of the BP-TiO_2-C composites. The Warburg coefficient σ, which is the slope of the plot between Z_{re} and $\omega^{-1/2}$, has been linearly fitted in Fig. 7b to evaluate the ionic diffusion coefficient. It is noted that the BP-TiO_2-C exhibits the smaller σ value, thereby suggesting the superior ionic diffusion property [12]. This result indicates that the TiO_2 can contribute the effectively enhancement on the lithium ion diffusion inside the active particles.

Fig. 7c and 7d present respectively the SEM images of BP-TiO_2-C and BP-C electrodes observed after 100 cycles at 1.0 A g^{-1}. The cracks on the surface of BP-TiO_2-C are apparently finer and narrower than those of BP-C, which denotes the crack with width of approximately 2 μm. From the SEM images of BP-TiO_2-C and BP-C electrodes under cross-sectional view (as shown in Fig. 7e and 7f), it is easy to find that the BP-C shows the more significant volumetric expansion. These results clearly evidence that the introduction of TiO_2 in BP-C composite can buffer the stress and restrict the volume expansion produced by BP. To further investigate the stability of the Ti-O-P bond, high-resolution XPS spectra of O 1s in BP-TiO_2-C and BP-C electrodes after 100 cycles at 1000 mA g^{-1} was measured and presented in Fig. S6. The C-O-P bond can be observed in both BP-TiO_2-C and BP-C with the almost equivalent intensity,

as shown in Fig. S6. The additional formed Ti-O-P bond could be still observed in BP-TiO_2-C composite with the enhanced reversibility, prolonged cycling life and structural stability. Therefore, it is suggested that the improved stability of the BP-TiO_2-C composite might be mainly attributed to the additional formed Ti-O-P bond in the present case study.

The outstanding-performance lithium-storage of the BP-TiO_2-C composite can be attributed to the cooperative mechanism between the components in the vigorous composite. Firstly, the well-uniformed TiO_2 can form Li_xTiO_2 after the initial discharge process, thus improving the electrochemical reaction with high electronic and ionic conductivity. Secondly, TiO_2 can effectively confine the aggregation of BP, homogenize the volume change and further relieve the structure stress during cycling. Thirdly, the strong Ti-O-P bonds not only enable the efficient interfacial charge transfer and improve the utilization of the active material, but also further stabilize the structure of composite. The synergetic combination of the above aspects leads to the synthesized BP-TiO_2-C composite having excellent electrochemical performance.

4. Conclusions

In summary, a ternary amorphous BP-TiO_2-C nanocomposite has been fabricated in the present work by one-step ball milling technology under argon as the LIBs anode material. The in-situ formed Li_XTiO_2 not only enhance the electronic and ionic transfer, but also homogenize the volume expansion, relieve the structural stress, maintain the structural stability. More importantly, the Ti-O-P bonds improve the utilization of active

material, the transfer of the interfacial electron and further stabilize the structure of composite. Overall, the synergetic effects of these superiorities enable the synthesized BP-TiO_2-C composite exhibits a high stable capacity of 1026 mAh g^{-1} at 500 mA g^{-1} after 200 cycles and 935.8 mAh g^{-1} at 2000 mA g^{-1} after 300 cycles. A reversible capacity of 947.4 mAh g^{-1} can be maintained even at the as high as 7.0 A g^{-1} current density, exhibiting excellent rate capacity. In addition, when fabricated as full cell with LCO cathode, the BP-TiO_2-C composite also shows a good capacity and cycle performance, indicating the great potential of the commercial application. Overall, this study shows a new strategy for developing the phosphorus-based anode material with high electrochemical performance.

Corresponding authors

[a*] E-mail: meouyang@scut.edu.cn, (L. Ouyang)
[c*] E-mail: xsyang@polyu.edu.hk, (X. Yang)

Conflicts of interest

The authors declare no conflict of financial interest.

Acknowledgements

We appreciate the financial support from the National Natural Science Foundation of China Projects (Nos. 51771075 and 51701171), Foundation for Innovative Research Groups of the National Natural Science Foundation of China (No. NSFC51621001), and Natural Science Foundation of Guangdong Province of China (No. 2016A030312011). L.Z. Ouyang is also grateful to the support from the Guangdong Province Universities and Colleges Pearl River Scholar Funded Scheme (2014).

Reference

[1] N. Nitta, F.X. Wu, J.T. Lee, G. Yushin, Li-ion battery materials: present and future, Mater. Today 2015, 18 (5), 252-264.

[2] L. Croguennec, M.R. Palacin, Recent achievements on inorganic electrode materials for lithium-ion batteries, J. Am. Chem. Soc. 2015, 137 (9), 3140-3156.

[3] C.M. Park, H.J. Sohn, Black phosphorus and its composite for lithium rechargeable batteries, Adv. Mater. 2007, 19 (18), 2465-2468.

[4] Y.J. Kim, Y. Park, A. Choi, N.S. Choi, J. Kim, J. Lee, J.H. Ryu, S.M. Oh, K.T. Lee, An amorphous red phosphorus/carbon composite as a promising anode material for sodium ion batteries, Adv. Mater. 2013, 25 (22), 3045-3049.

[5] J. Sun, G.Y. Zheng, H.W. Lee, N. Liu, H.T. Wang, H.B. Yao, W.S. Yang, Y. Cui, Formation of stable phosphorus-carbon bond for enhanced performance in black phosphorus nanoparticle-graphite composite battery anodes, Nano Lett. 2014, 14 (8), 4573-4580.

[6] W.L. Liu, X.X. Yuan, X.B. Yu, A core-shell structure of polydopamine-coated phosphorus-carbon nanotube composite for high-performance sodium-ion batteries, Nanoscale 2018, 10 (35), 16675-16682.

[7] H.W. Liu, Y.Q. Zou, L. Tao, Z.L. Ma, D.D. Liu, P. Zhou, H.B. Liu, S.Y. Wang, Sandwiched thin-film anode of chemically bonded black phosphorus/graphene hybrid for lithium-ion battery, Small 2017, 13 (33), 1700758.

[8] G.C. Guo, X.L. Wei, D. Wang, Y.P. Luo, L.M. Liu, Pristine and defect-containing phosphorene as promising anode materials for rechargeable Li batteries, J. Mater.

Chem. A 2015, 3 (21), 11246-11252.

[9] R.J. Meng, J.M. Huang, Y.T. Feng, L.H. Zu, C.X. Peng, L.R. Zheng, L. Zheng, Z.B. Chen, G.L. Liu, B.J. Chen, Y.L. Mi, J.H. Yang, Black phosphorus quantum dot/Ti_3C_2 MXene nanosheet composites for efficient electrochemical lithium/sodium-ion storage, Adv. Energy Mater. 2018, 8 (26), 1801514.

[10] L. Pan, X.D. Zhu, K.N. Sun, Y.T. Liu, X.M. Xie, X.Y. Ye, Molecular level distribution of black phosphorus quantum dots on nitrogen doped graphene nanosheets for superior lithium storage, Nano Energy 2016, 30, 347-354.

[11] Y.H. Liu, A.Y. Zhang, C.F. Shen, Q.Z. Liu, X. Cao, Y.Q. Ma, L. Chen, C. Lau, T.C. Chen, F. Wei, C.W. Zhou, Red phosphorus nanodots on reduced graphene oxide as a flexible and ultra-fast anode for sodium-ion batteries, ACS Nano 2017, 11 (6), 5530-5537.

[12] J.B. Zhou, Z.H. Jiang, S.W. Niu, S.S. Zhu, J. Zhou, Y.C. Zhu, J.W. Liang, D.D. Han, K.L. Xu, L.Q. Zhu, X.J. Liu, G.M. Wang, Y.T. Qian, Self-standing hierarchical P/CNTs@rGO with unprecedented capacity and stability for lithium and sodium storage, Chem 2018, 4 (2), 372-385.

[13] T. Yuan, J. Ruan, C.X. Peng, H. Sun, Y.P. Pang, J.H. Yang, Z.F. Ma, S.Y. Zheng, 3D red phosphorus/sheared CNT sponge for high performance lithium-ion battery anodes, Energy Storage Mater. 2018, 13, 267-273.

[14] J.F. Ruan, Y.P. Pang, S.N. Luo, T. Yuan, C.X. Peng, J.H. Yang, S.Y. Zheng, Ultrafine red P nanoconfined between expanded graphene sheets for high-performance lithium-ion batteries, J. Mater. Chem. A 2018, 6 (42), 20804-20812.

[15] G.L. Xu, Z.H. Chen, G.M. Zhong, Y.Z. Liu, Y. Yang, T.Y. Ma, Y. Ren, X.B. Zuo, X.H. Wu, X.Y. Zhang, K. Amine, Nanostructured black phosphorus/ketjenblack-multiwalled carbon nanotubes composite as high performance anode material for sodium-ion batteries, Nano Lett. 2016, 16 (6), 3955-3965.

[16] D. Deng, M.G. Kim, J.Y. Lee, J. Cho, Green energy storage materials: nanostructured TiO_2 and Sn-based anodes for lithium-ion batteries, Energy Environ. Sci. 2009, 2 (8), 818-837.

[17] J.S. Chen, Y.L. Tan, C.M. Li, Y.L. Cheah, D.Y. Luan, S. Madhavi, F.Y. Boey, L.A. Archer, X.W. Lou, Constructing hierarchical spheres from large ultrathin anatase TiO_2 nanosheets with nearly 100% exposed (001) facets for fast reversible lithium storage, J. Am. Chem. Soc. 2010, 132 (17), 6124-6130.

[18] C.H. Sun, X.H. Yang, J.S. Chen, Z. Li, X.W. Lou, C.Z. Li, S.C. Smith, G.Q. Lu, H.G. Yang, Higher charge/discharge rates of lithium-ions across engineered TiO_2 surfaces leads to enhanced battery performance, Chem. Commun. 2010, 46 (33), 6129-6131.

[19] Z.L. Li, H.L. Zhao, P.P. Lv, Z.J. Zhang, Y. Zhang, Z.H. Du, Y.Q. Teng, L.N. Zhao, Z.M. Zhu, Watermelon-like structured SiO_x-TiO_2@C nanocomposite as a high-performance lithium-ion battery anode, Adv. Funct. Mater. 2018, 28 (31), 1605711.

[20] J.Y. Cheong, C. Kim, J.W. Jung, T.G. Yun, D.Y. Youn, S.H. Cho, K.R. Yoon, H.Y. Jang, S.W. Song, I.D. Kim, Incorporation of amorphous TiO_2 into one-dimensional SnO_2 nanostructures as superior anodes for lithium-ion batteries, J. Power Sources 2018, 400, 485-492.

[21] T.B. Song, H. Chen, Z. Li, Q.J. Xu, H.M. Liu, Y.G. Wang, Y.Y. Xia, Creating an Air-Stable Sulfur-Doped Black Phosphorus-TiO_2 Composite as High-Performance Anode Material for Sodium-Ion Storage, Adv. Funct. Mater., 22 (29), 1900535.

[22] J.X. Song, Z.X. Yu, M.L. Gordin, S. Hu, R. Yi, D.H. Tang, T. Walter, M. Regula, D. Choi, X.L. Li, A. Manivannan, D.H. Wang, Chemically bonded phosphorus/graphene hybrid as a high performance anode for sodium-ion batteries, Nano Lett. 2014, 14 (11), 6329-6335.

[23] F.C. Zhou, L.Z. Ouyang, M.Q. Zeng, J.W. Liu, H. Wang, H.Y. Shao, M. Zhu, Growth mechanism of black phosphorus synthesized by different ball milling techniques, J. Alloy. Compd. 2019, 784, 339-346.

[24] T. Nilges, M. Kersting, T. Pfeifer, A fast low-pressure transport route to large black phosphorus single crystals, J. Solid State Chem. 2008, 181 (8), 1707-1711.

[25] M. Köpf, N. Eckstein, D. Pfister, C. Grotz, I. Krüger, M. Greiwe, T. Hansen, H. Kohlmann, T. Nilges, Access and in situ growth of phosphorene-precursor black phosphorus, J. Cryst. Growth 2014, 405, 6-10.

[26] L.M. Malard, M.A. Pimenta, G. Dresselhaus, M.S. Dresselhaus, Raman spectroscopy in graphene, Phys. Rep. 2009, 473 (5-6), 51-87.

[27] W.F. Zhang, Y.L. He, M.S. Zhang, Z. Yin, Q. Chen, Raman scattering study on anatase TiO_2 nanocrystals, J. Phys. D Appl. Phys. 2000, 33 (8), 912-916.

[28] Y.F. Luo, H.C. Wu, L. Liu, Q.Q. Li, K.L. Jiang, S.S. Fan, J. Li, J.P. Wang, TiO_2-nanocoated black phosphorus electrodes with improved electrochemical performance, ACS Appl. Mater. Interfaces 2018, 10 (42), 36058-36066.

[29] Z.X. Yu, J.X. Song, M.L. Gordin, R. Yi, D.H. Tang, D.H. Wang, Phosphorus-graphene nanosheet hybrids as lithium-ion anode with exceptional high-temperature cycling stability, Adv. Sci. 2015, 2 (1-2), 1400020.

[30] W.J. Li, S.L. Chou, J.Z. Wang, H.K. Liu, S.X. Dou, Significant enhancement of the cycling performance and rate capability of the P/C composite via chemical bonding (P–C), J. Mater. Chem. A 2016, 4 (2), 505-511.

[31] J. Sun, H.W. Lee, M. Pasta, Y.M. Sun, W. Liu, Y.B. Li, H.R. Lee, N. Liu, Y. Cui, Carbothermic reduction synthesis of red phosphorus-filled 3D carbon material as a high-capacity anode for sodium ion batteries, Energy Storage Mater. 2016, 4, 130-136.

[32] T. Wu, J.C. Fan, Q.X. Li, P.H. Shi, Q.J. Xu, Y.L. Min, Palladium nanoparticles anchored on anatase titanium dioxide-black phosphorus hybrids with heterointerfaces: highly electroactive and durable catalysts for ethanol electrooxidation, Adv. Energy Mater. 2018, 8 (1), 1701799.

[33] N.O. Gopal, H.H. Lo, T.F. Ke, C.H. Lee, C.C. Chou, J.D. Wu, S.C. Sheu, S.C. Ke, Visible light active phosphorus-doped TiO_2 nanoparticles: an EPR evidence for the enhanced charge separation, J. Phys. Chem. C 2012, 116 (30), 16191-16197.

[34] P.X. Li, X. Guo, S.J. Wang, R. Zang, X.M. Li, Z.M. Man, P. Li, S.S. Liu, Y.H. Wu, G.X. Wang, Two-dimensional $Sb@TiO_{2-x}$ nanoplates as a high-performance anode material for sodium-ion batteries, J. Mater. Chem. A 2019, 7 (6), 2553-2559.

[35] W.C. Chang, K.W. Tseng, H.Y. Tuan, Solution synthesis of iodine-doped red phosphorus nanoparticles for lithium-ion battery anodes, Nano Lett. 2017, 17 (2),

1240-1247.

[36] X.Y. Li, G. Chen, Z.Y. Le, X.R. Li, P. Nie, X.Y. Liu, P.C. Xu, H.B. Wu, Z. Liu, Y.F. Lu, Well-dispersed phosphorus nanocrystals within carbon via high-energy mechanical milling for high performance lithium Storage, Nano Energy 2019, 59, 464-471.

[37] T. Xu, D.H. Li, S. Chen, Y.Y. Sun, H.W. Zhang, Y.Z. Xia, D.J. Yang, Nanoconfinement of red phosphorus nanoparticles in seaweed-derived hierarchical porous carbonaceous fibers for enhanced lithium ion storage, Chem. Eng. J. 2018, 345, 604-610.

[38] L. Sun, Y. Zhang, D.Y. Zhang, Y.H. Zhang, Amorphous red phosphorus nanosheets anchored on graphene layers as high performance anodes for lithium ion batteries, Nanoscale 2017, 9 (46), 18552-18560.

[39] L. Sun, Y. Zhang, D.Y. Zhang, J.G. Liu, Y.H. Zhang, Amorphous red phosphorus anchored on carbon nanotubes as high performance electrodes for lithium ion batteries, Nano Research 2018, 11 (5), 2733-2745.

[40] Y. Zhang, H.W. Wang, Z.Z. Luo, H.T. Tan, B. Li, S.N. Sun, Z. Li, Y. Zong, Z.C. Xu, Y.H. Yang, K.A. Khor, Q.Y. Yan, An air-stable densely packed phosphorene-graphene composite toward advanced lithium storage properties, Adv. Energy Mater. 2016, 6 (12), 1600453.

[41] L. Chen, G.M. Zhou, Z.B. Liu, X.M. Ma, J. Chen, Z.Y. Zhang, X.L. Ma, F. Li, H.M. Cheng, W.C. Ren, Scalable clean exfoliation of high-quality few-layer black phosphorus for a flexible lithium ion battery, Adv. Mater. 2016, 28 (3), 510-517.

[42] Y. Liu, Q. Liu, A. Zhang, J. Cai, X. Cao, Z. Li, P.D. Asimow, C.W. Zhou, Room-temperature pressure synthesis of layered black phosphorus-graphene composite for sodium-ion battery anodes, ACS Nano 2018, 12 (8), 8323-8329.

[43] T. Liang, R.Z. Hu, H.P. Zhang, H.Y. Zhang, H. Wang, Y.P. Ouyang, J. Liu, L.C. Yang, M. Zhu, A scalable ternary SnO_2–Co–C composite as a high initial coulombic efficiency, large capacity and long lifetime anode for lithium ion batteries, J. Mater. Chem. A 2018, 6 (16), 7206-7220.

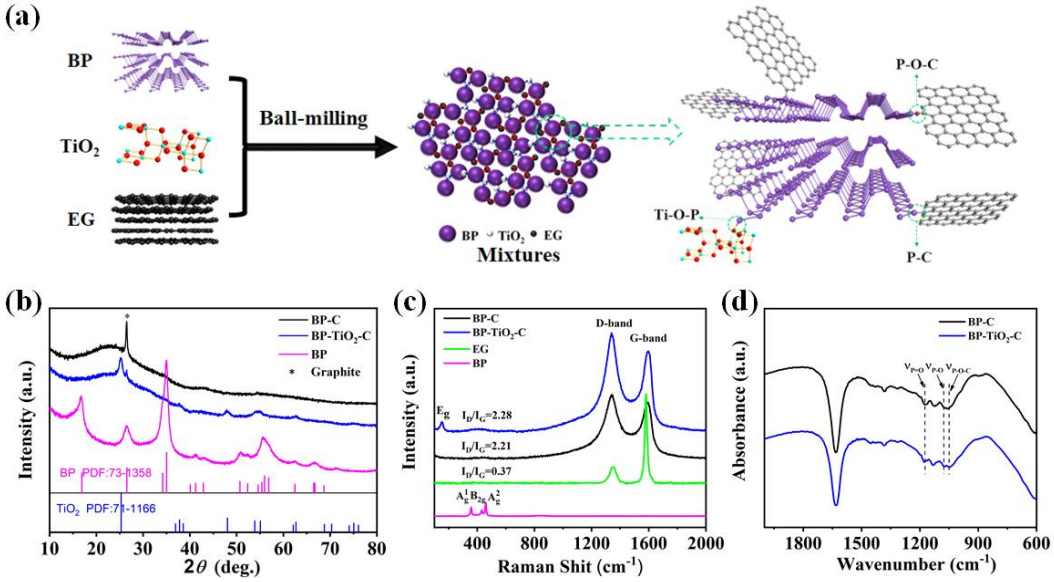

Fig. 1. a) Schematic illustration of the fabrication of the BP-TiO_2-C composite, b) the XRD patterns of BP-TiO_2-C, BP-C and BP, c) Raman spectra of BP-TiO_2-C, BP-C, BP and EG, and d) FTIR spectra of BP-TiO_2-C and BP-C composites.

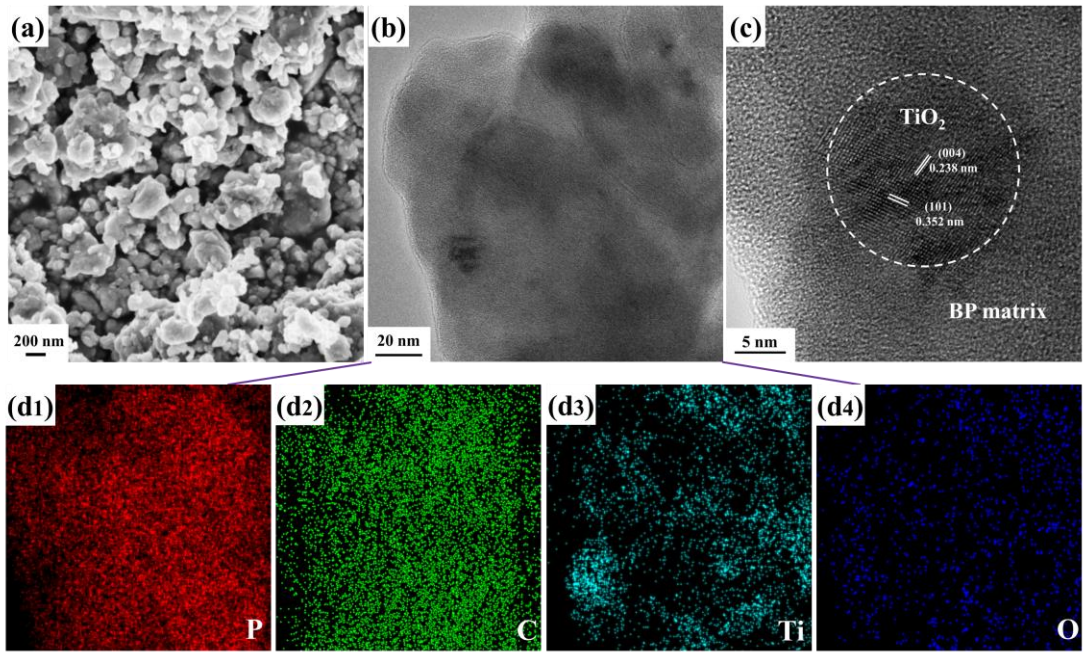

Fig. 2. a) SEM image of the BP-TiO_2-C composite, b) TEM image and c) HRTEM images of BP-TiO_2-C, d1-d4) the element mapping images of BP-TiO_2-C composite.

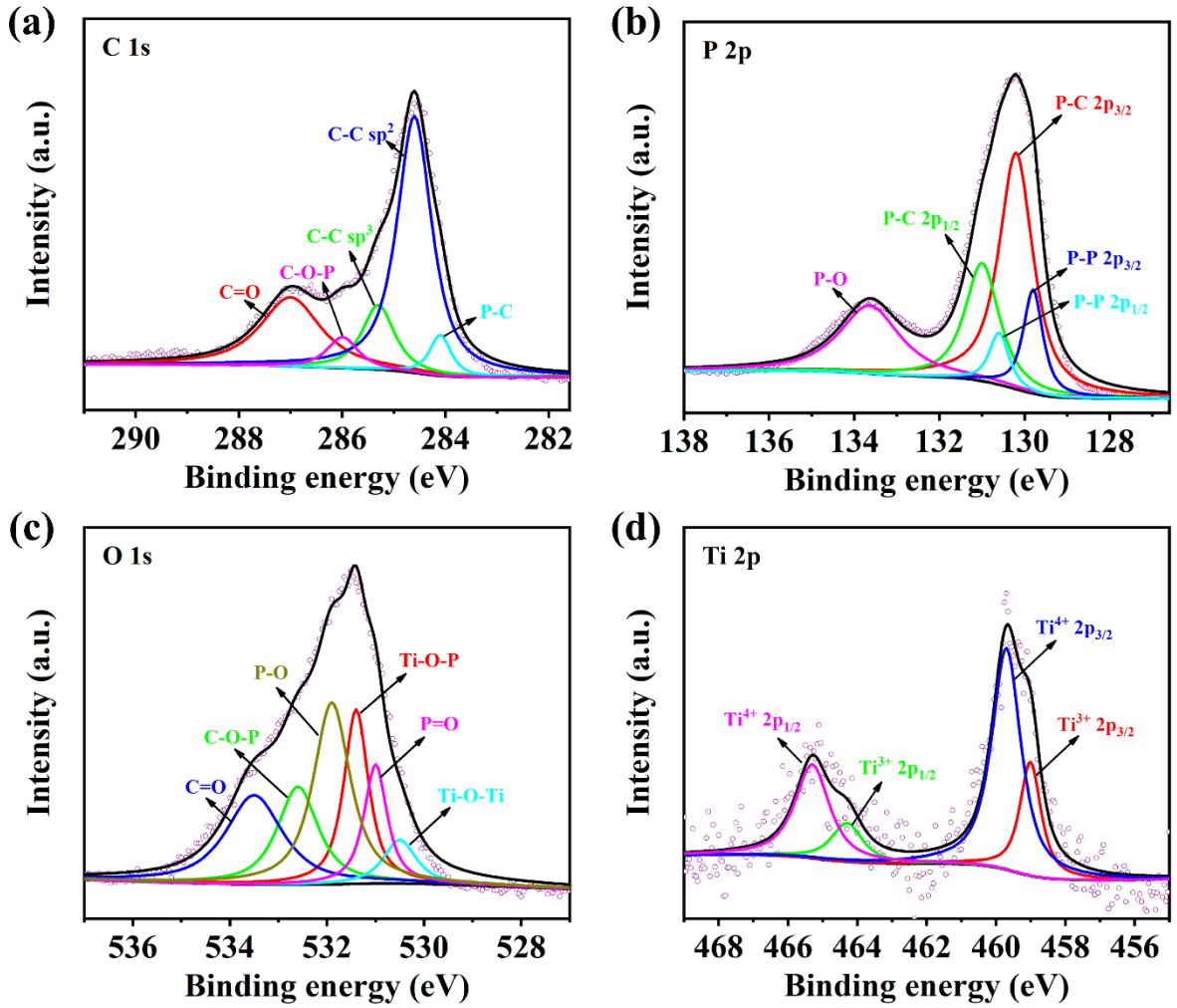

Fig. 3. High-resolution XPS spectra of a) C 1s, b) P 2p, c) O 1s, and d) Ti 2p in the BP-TiO_2-C composite.

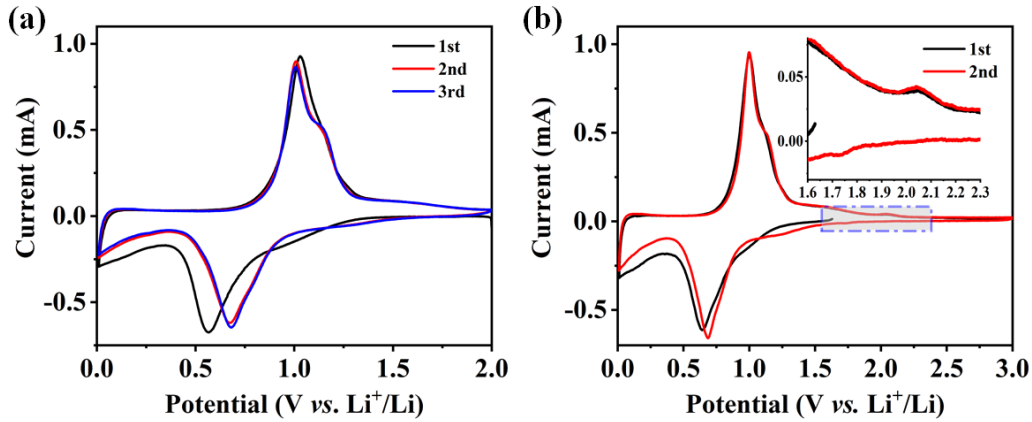

Fig. 4. CV curves of BP-TiO_2-C electrode with different voltage range of a) 0.01-2.00 V (vs. Li^+/Li), b) 0.01-3.00 V (vs. Li^+/Li). The inset in (b) showing the partial-enlarged CV curves in the dashed area.

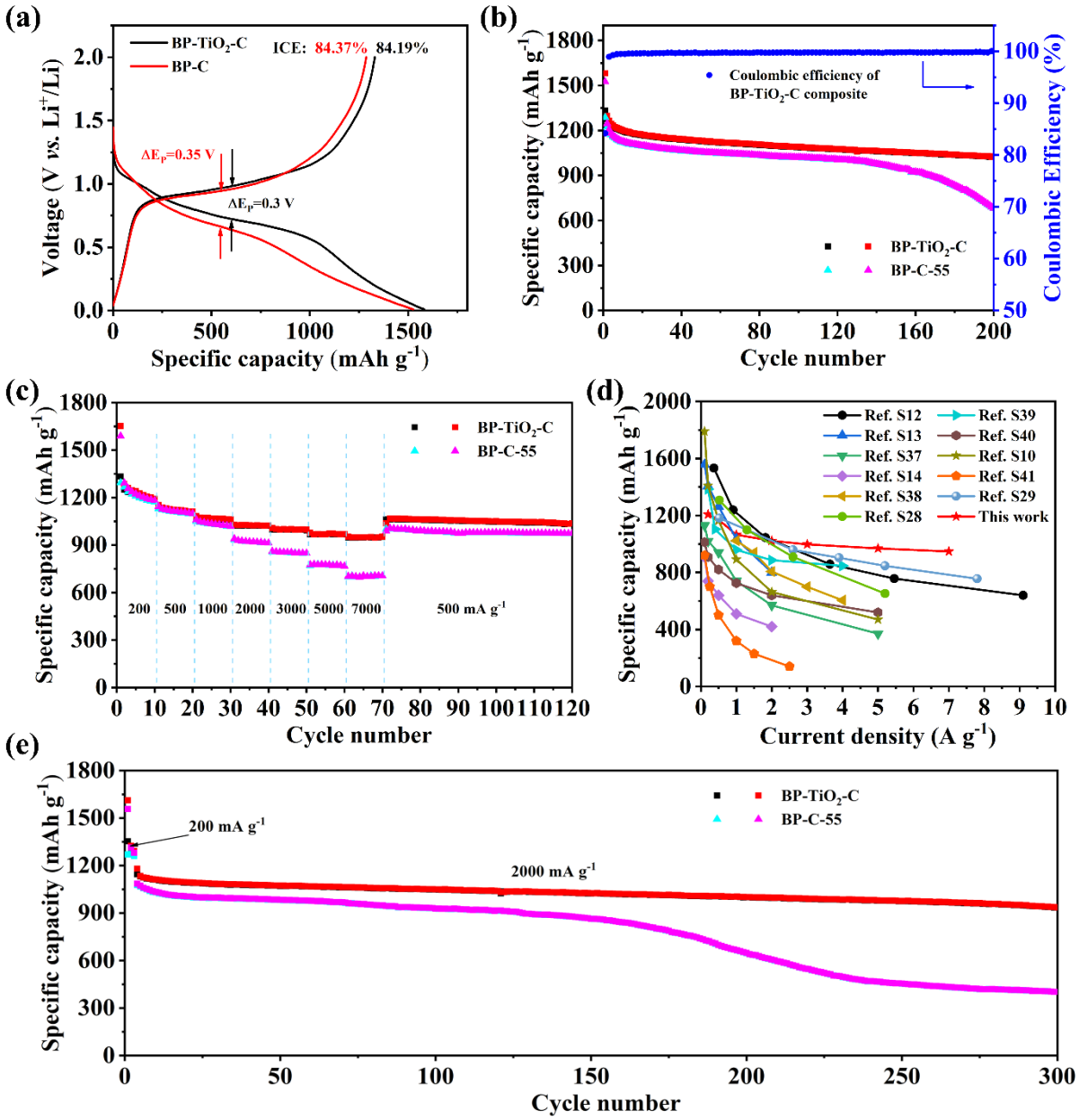

Fig. 5. a) The charge-discharge curves at 500 mA g^{-1} in the first cycle, b) cycling performances at 500 mA g^{-1}, c) rate capabilities, d) The rate capabilities of recent reported P-based anode materials for LIBs at various current densities, and e) long cycling performance at 2000 mA g^{-1} of BP-TiO_2-C and BP-C electrodes.

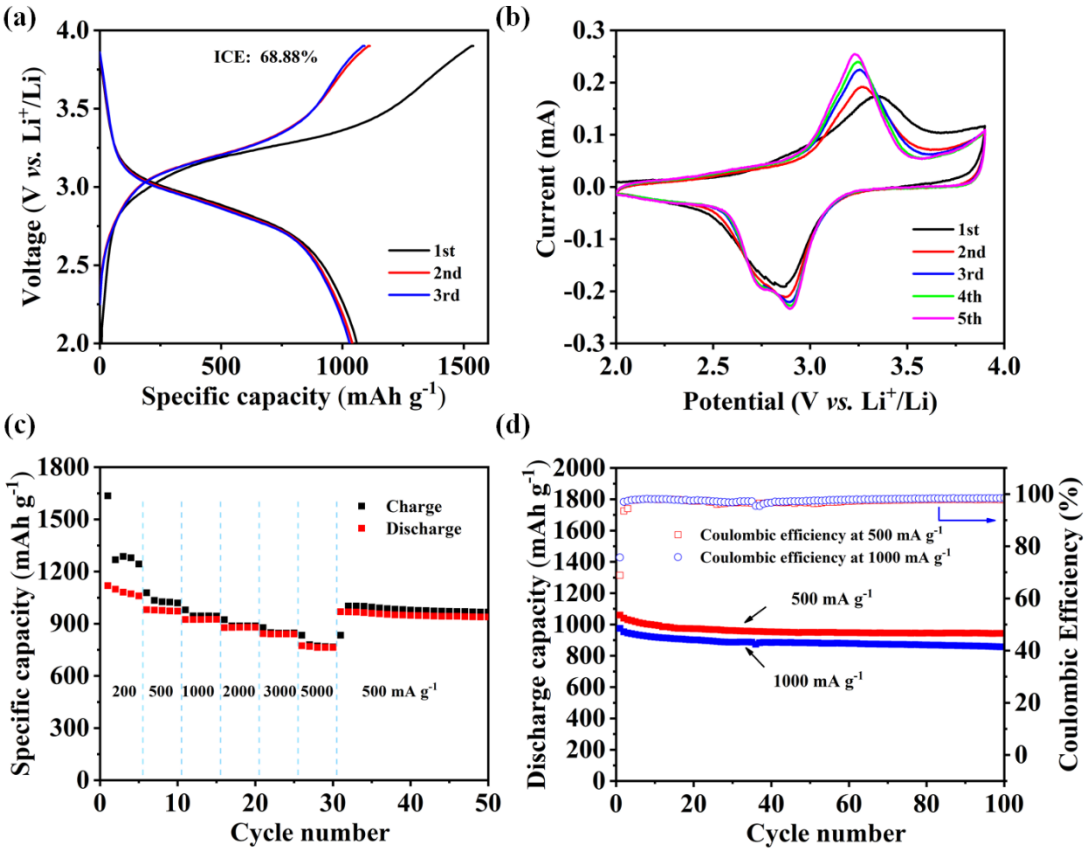

Fig. 6. The electrochemical performance of LCO|BP-TiO_2-C full cell. a) The charge/discharge profile at current density of 500 mA g^{-1}, b) CV curves, c) rate performance, d) cycling performance.

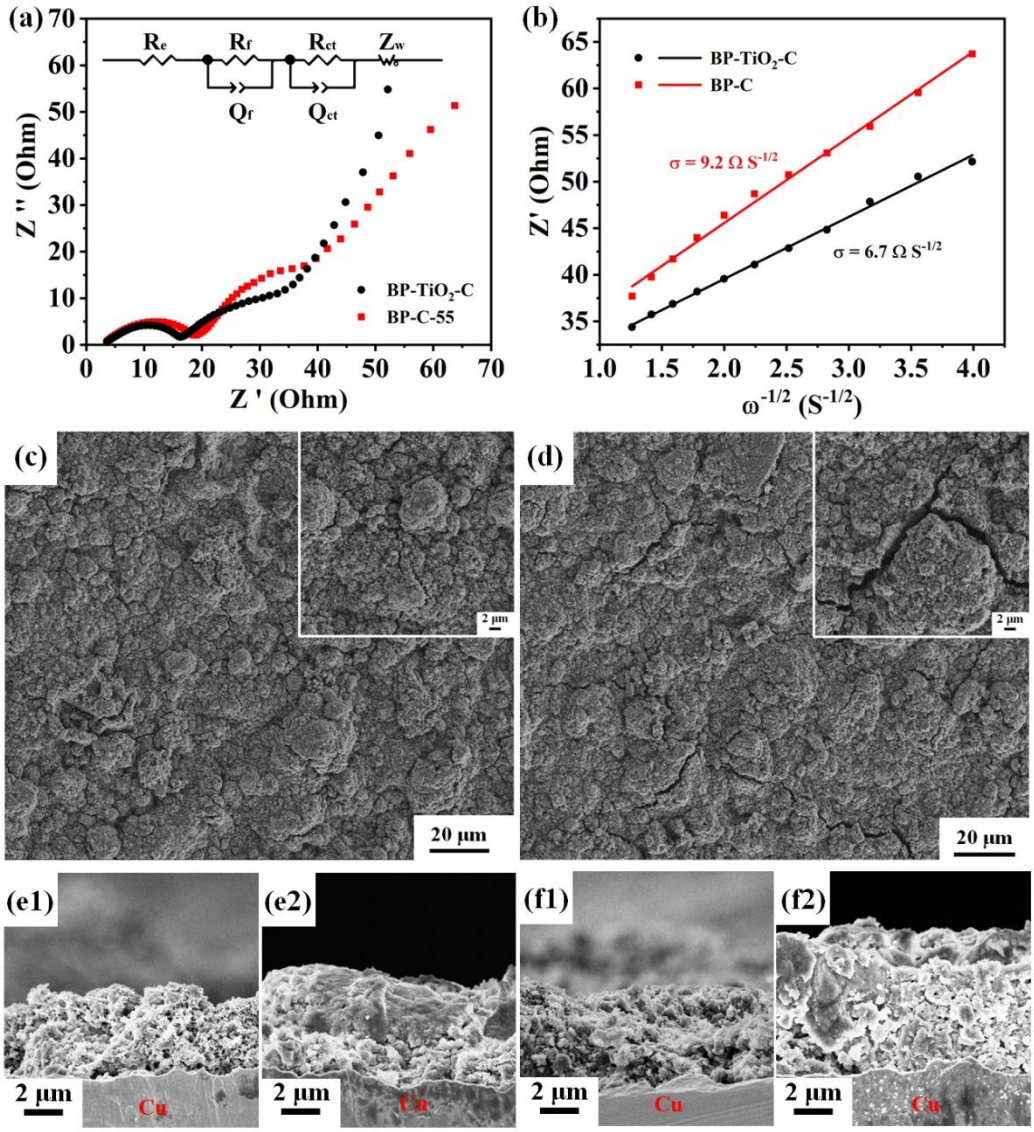

Fig. 7. a) Electrochemical impedance spectra of 100 cycled BP-TiO_2-C and BP-C electrodes at discharge states of 0.01V. b) Relationship between Z_{re} and $\omega^{-1/2}$. The SEM images for the surface morphologies of c) BP-TiO_2-C and d) BP-C electrodes, respectively, at 1000 mA g^{-1} after 100 cycles. e, f) The SEM images under cross-sectional view of the BP-TiO_2-C and BP-C electrodes before and after 100 cycles at 1000 mA g^{-1}. e1) before cycle and e2) after 100 cycles of BP-TiO_2-C; f1) before cycle and f2) after 100 cycles of BP-C.

Supplementary Material

Chemical Bonding Black Phosphorus with TiO_2 and Carbon toward High-Performance Lithium Storage

Fengchen Zhou[a], Liuzhang Ouyang[a,b*], Jiangwen Liu[a], Xu-Sheng Yang[c,d*], Min Zhu[a]

[a] School of Materials Science and Engineering, Guangdong Provincial Key Laboratory of Advanced Energy Storage Materials, South China University of Technology, Guangzhou, 510641, China. Email: meouyang@scut.edu.cn

[b] China-Australia Joint Laboratory for Energy & Environmental Materials, Key Laboratory of Fuel Cell Technology of Guangdong Province, Guangzhou, 510641, China

[c] Advanced Manufacturing Technology Research Centre, Department of Industrial and Systems Engineering, The Hong Kong Polytechnic University, Hung Hom, Kowloon, Hong Kong, China. Email: xsyang@polyu.edu.hk

[d] Hong Kong Polytechnic University Shenzhen Research Institute, Shenzhen 518057, China

*Corresponding authors.
[a*] E-mail: meouyang@scut.edu.cn, (L. Ouyang)
[c*] E-mail: xsyang@polyu.edu.hk, (X. Yang)

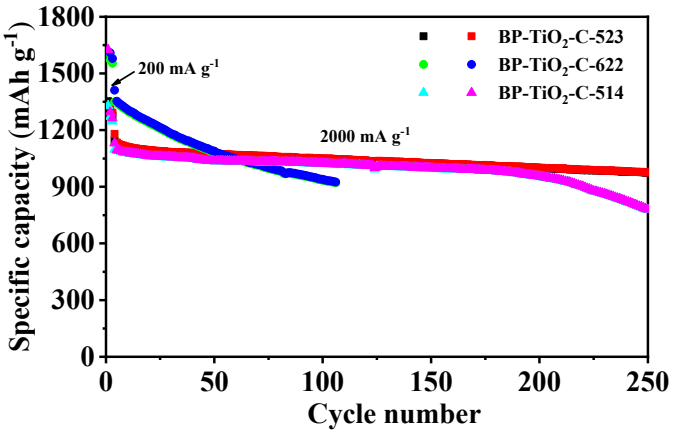

Fig.S1 The preliminary cycling performances of BP-TiO_2-C composites. BP: TiO_2: C with weight ratios of 5:1:4, 5:2:3 and 6:2:2 are labeled as BP-TiO_2-C-514, BP-TiO_2-C-523 and BP-TiO_2-C-622, respectively.

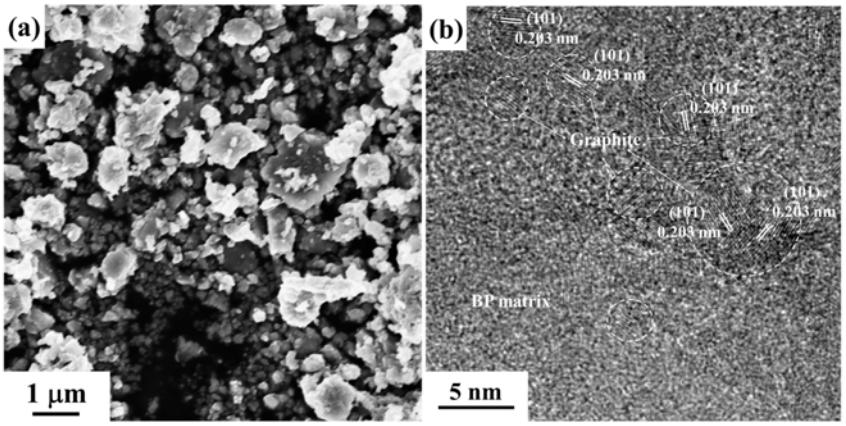

Fig. S2 (a) SEM and (b) HRTEM images of the BP-C composite.

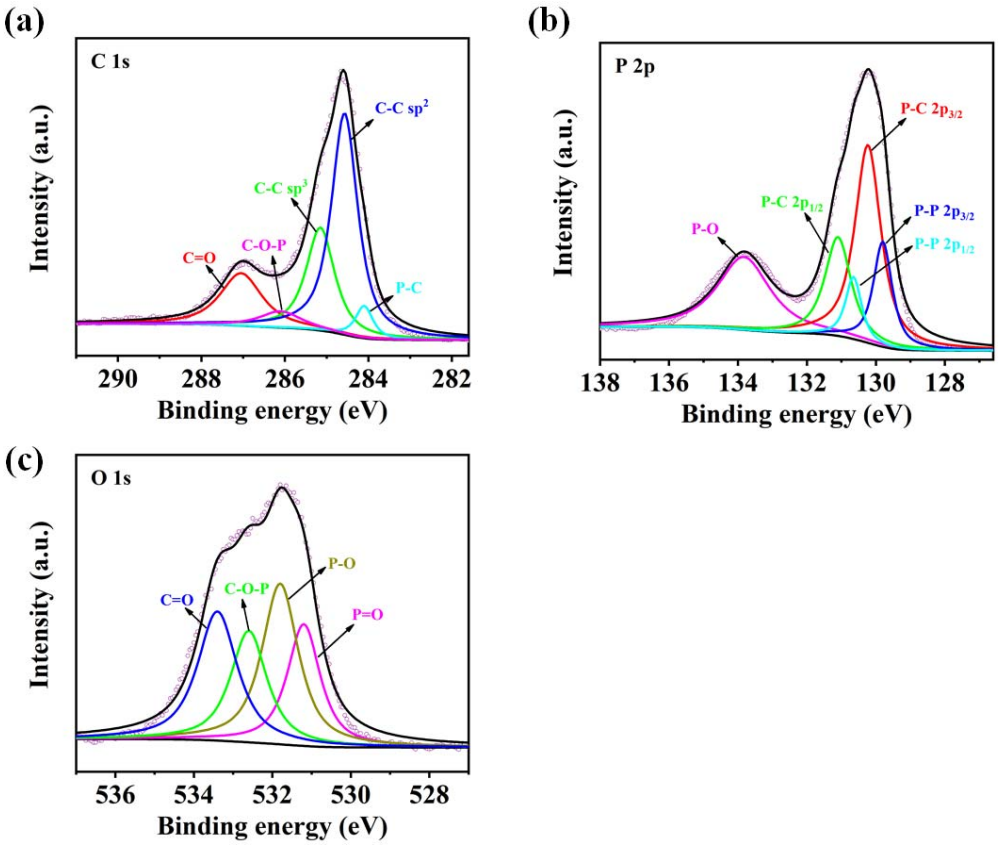

Fig. S3 High-resolution XPS spectra of (a) C 1s, (b) P 2p, and (c) O 1s in the BP-C composite.

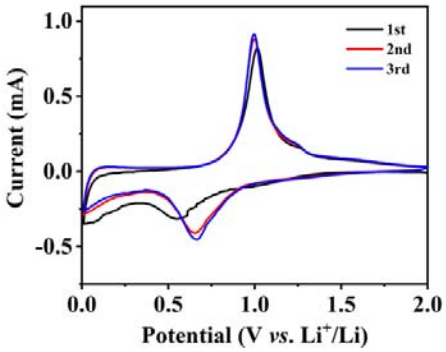

Fig. S4 CV curves of BP-C electrode.

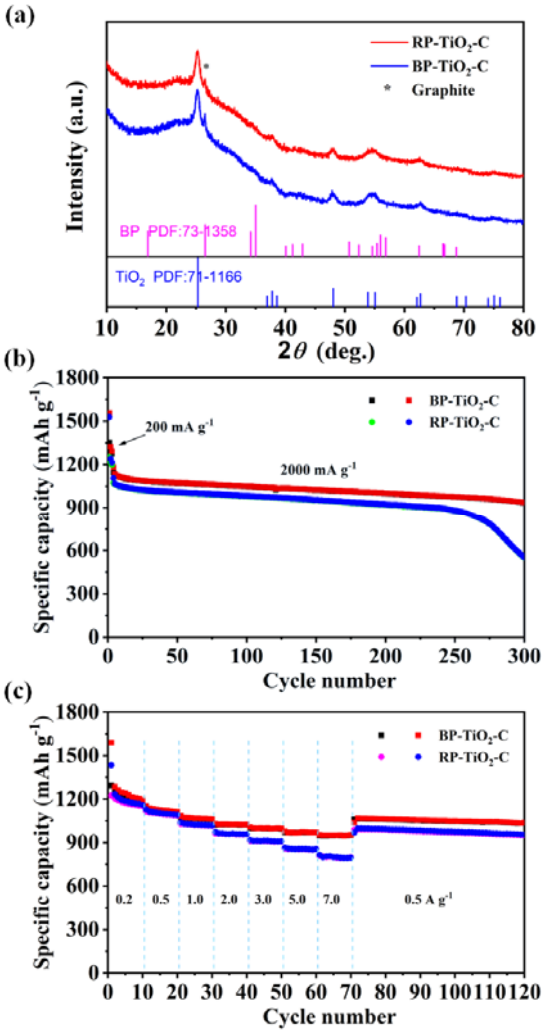

Fig. S5 (a) The XRD patterns of BP-TiO_2-C and RP-TiO_2-C, (b) cycle performances at 2000 mA g^{-1}, (c) rate capabilities of BP-TiO_2-C and RP-TiO_2-C electrodes.

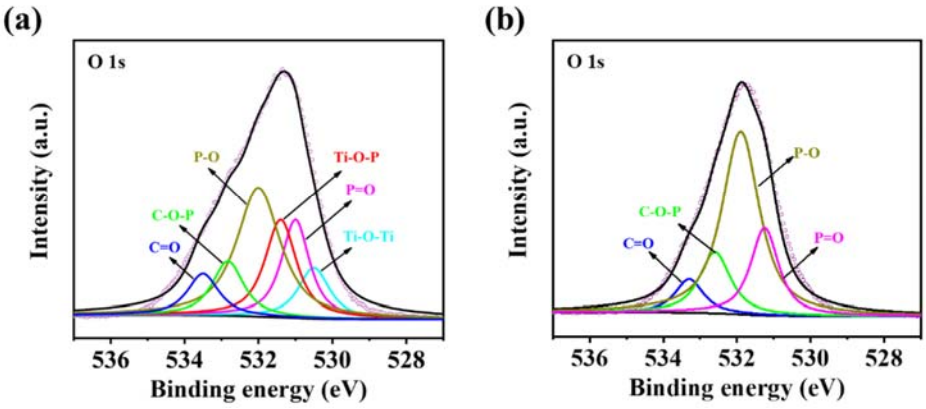

Fig. S6 High-resolution XPS spectra of O 1s in the (a) BP-TiO_2-C and (b) BP-C electrodes after 100 cycles at 1000 mA g^{-1}, respectively.

Table S1 Comparison of this work with previously reported P-based composites (the capacity based on the weight of composite).

Sample	P loading	Current densities	Reversible capacity	Initial coulombic efficiency	Cyclic performance	Reference
BP-TiO_2-C	70%	500 mA g^{-1}	1331.1 mAh g^{-1}	84.19%	Capacities of ~1026 mAh g^{-1} after 200 cycles at 500 mAg^{-1} and 935.8 mAh g^{-1} after 300 cycles at 2000 mA g^{-1}	This work
BP-Gr	80%	100 mA g^{-1}	920 mAh g^{-1}		Capacity of 402 after 500 cycles at 500 mA g^{-1}	1
BP-G	46.26%	0.52 mA g^{-1}	1101.9 mAh g^{-1}	85.5%	Capacity of 855 after 100 cycles at 520 mA g^{-1}	2
P-SCNT composite	36%	100 mA g^{-1}	1621.1 mAh g^{-1}	77%	Capacities of ~1398.5 mAh g^{-1} after 200 cycles at 100 mAg^{-1} and ~782 mAh g^{-1} after 3000 cycles at 2 A g^{-1}	3
P@HPCE-3/2	36.7%	1000 mA g^{-1}	830 mAh g^{-1}	65.4%	Capacity of 636.7 after 100 cycles at 1000 mA g^{-1}	4
P@expanded-G50	31.5%	100 mA g^{-1}	965.1 mAh g^{-1}	64%	Capacity of 1010 after 500 cycles at 100 mA g^{-1}	5
P/graphene	80%	200 mA g^{-1}	1555 mAh g^{-1}	72%	Capacity of 1024 after 100 cycles at 200 mA g^{-1}	6
P@CNT	72%	200 mA g^{-1}	1451.2 mAh g^{-1}	67%	Capacity of 960 after 120 cycles at 200 mA g^{-1}	7
PG-SPS		100 mA g^{-1}	1302 mAh g^{-1}	60.2%	Capacity of 725 after 200 cycles at 500 mA g^{-1}	8
BPQDs-NG	66.22%	500 mA g^{-1}	1583 mAh g^{-1}	76.8%	Capacity of 1271 after 100 cycles at 500 mA g^{-1}	9

P-G	70%	260 mA g^{-1}	1477 mAh g^{-1}	84%	Capacity of 898 after 300 cycles at 260 mA g^{-1}	10

Reference:

[1] L. Chen, G.M. Zhou, Z.B. Liu, X.M. Ma, J. Chen, Z.Y. Zhang, X.L. Ma, F. Li, H.M. Cheng, W.C. Ren, Scalable clean exfoliation of high-quality few-layer black phosphorus for a flexible lithium ion battery, Adv. Mater. 2016, 28 (3), 510-517.

[2] J. Sun, G.Y. Zheng, H.W. Lee, N. Liu, H.T. Wang, H.B. Yao, W.S. Yang, Y. Cui, Formation of stable phosphorus-carbon bond for enhanced performance in black phosphorus nanoparticle-graphite composite battery anodes, Nano Lett. 2014, 14 (8), 4573-4580.

[3] T. Yuan, J. Ruan, C.X. Peng, H. Sun, Y.P. Pang, J.H. Yang, Z.F. Ma, S.Y. Zheng, 3D red phosphorus/sheared CNT sponge for high performance lithium-ion battery anodes, Energy Storage Mater. 2018, 13, 267-273.

[4] T. Xu, D.H. Li, S. Chen, Y.Y. Sun, H.W. Zhang, Y.Z. Xia, D.J. Yang, Nanoconfinement of red phosphorus nanoparticles in seaweed-derived hierarchical porous carbonaceous fibers for enhanced lithium ion storage, Chem. Eng. J. 2018, 345, 604-610.

[5] J.F. Ruan, Y.P. Pang, S.N. Luo, T. Yuan, C.X. Peng, J.H. Yang, S.Y. Zheng, Ultrafine red P nanoconfined between expanded graphene sheets for high-performance lithium-ion batteries, J. Mater. Chem. A 2018, 6 (42), 20804-20812.

[6] L. Sun, Y. Zhang, D.Y. Zhang, Y.H. Zhang, Amorphous red phosphorus nanosheets anchored on graphene layers as high performance anodes for lithium ion batteries, Nanoscale 2017, 9 (46), 18552-18560.

[7] L. Sun, Y. Zhang, D.Y. Zhang, J.G. Liu, Y.H. Zhang, Amorphous red phosphorus anchored on carbon nanotubes as high performance electrodes

for lithium ion batteries, Nano Research 2018, 11 (5), 2733-2745.

[8] Y. Zhang, H.W. Wang, Z.Z. Luo, H.T. Tan, B. Li, S.N. Sun, Z. Li, Y. Zong, Z.C. Xu, Y.H. Yang, K.A. Khor, Q.Y. Yan, An air-stable densely packed phosphorene-graphene composite toward advanced lithium storage properties, Adv. Energy Mater. 2016, 6 (12), 1600453.

[9] L. Pan, X.D. Zhu, K.N. Sun, Y.T. Liu, X.M. Xie, X.Y. Ye, Molecular level distribution of black phosphorus quantum dots on nitrogen doped graphene nanosheets for superior lithium storage, Nano Energy 2016, 30, 347-354.

[10] Z.X. Yu, J.X. Song, M.L. Gordin, R. Yi, D.H. Tang, D.H. Wang, Phosphorus-graphene nanosheet hybrids as lithium-ion anode with exceptional high-temperature cycling stability, Adv. Sci. 2015, 2 (1-2), 1400020.